Pure Appl. Geophys.

DOI 10.1007/s00024-015-1103-0

Pure and Applied Geophysics

# Analysis of Foreshock Sequences in California and Implications for Earthquake Triggering

Xiaowei Chen[1] and Peter M. Shearer[2]

*Abstract*—We analyze foreshock activity in California and compare observations with simulated catalogs based on a branching aftershock-triggering model. We first examine foreshock occurrence patterns for isolated $M \geq 5$ earthquakes in southern California from 1981 to 2011 and in northern California from 1984 to 2009. Among the 64 $M \geq 5$ mainshocks, excluding 3 swarms and 3 doubles, 53 % of the rest are preceded by at least one foreshock within 30 days and 5 km. Foreshock occurrence appears correlated with mainshock faulting type and depth. Foreshock area is correlated with the magnitude of the largest foreshock and the number of foreshocks, however, it is not correlated with mainshock magnitude. We then examine the occurrence pattern of all seismicity clusters without a minimum magnitude requirement, and the possibility that they are "foreshocks" of larger mainshocks. Only about 30 % of the small clusters lead to a larger cluster. About 66 % of the larger clusters have foreshock activities, and the spatial distribution pattern is similar to $M \geq 5$ mainshocks, with lower occurrence rates in the Transverse Range and central California and higher occurrence rates in the Eastern California Shear Zone and the Bay Area. These results suggest that foreshock occurrence is largely controlled by the regional tectonic stress field and fault zone properties. In special cases, foreshock occurrence may be useful for short-term forecasting; however, foreshock properties are not reliably predictive of the magnitude of the eventual "mainshock". Comparison with simulated catalogs suggest that the "swarmy" features and foreshock occurrence rate in the observed catalogs are not well reproduced from common statistical models of earthquake triggering.

## 1. Introduction

Mogi (1963) distinguished three main types of earthquake sequences: (1) mainshocks with both foreshocks and aftershocks; (2) mainshocks and aftershocks but no foreshocks; and (3) earthquake swarms that lack clear mainshocks. There have been studies of the triggering process involved in each category. Aftershocks are usually assumed triggered by dynamic or static stress changes imposed by the mainshocks (e.g., Toda *et al.* 2012), and earthquake swarms are thought to result from underlying crustal transient processes (e.g., Vidale and Shearer 2006; Chen *et al.* 2012). Foreshocks are of great interest because of their possible triggering role and predictive value, but their relationship to mainshocks is still poorly understood. The successful evacuation prior to the 1975 M7.3 Haicheng earthquake is a promising example for earthquake prediction; however, many mainshocks occur abruptly without foreshocks (e.g., the 2004 Parkfield earthquake), or the foreshocks are only recognized retrospectively (e.g., the 1992 Landers earthquake) Mignan (2014).

Two models have been suggested to explain foreshock occurrence: (1) "rupture model", where foreshocks and aftershocks can be explained with a common triggering model, as indicated by statistical tests of California seismicity Felzer *et al.* (2004), therefore, the mainshock is just an accidentally larger aftershock; (2) "pre-slip model", where foreshocks are triggered by quasi-static slip occurring within the mainshock nucleation zone, and foreshock properties are possibly predictive of mainshock magnitude (Dodge *et al.* 1996). Dodge *et al.* (1996) reported scaling of foreshock area with mainshock magnitude, which is similar to the scaling relationship of the proposed nucleation phase of Ellsworth and Beroza (1995). However, Felzer *et al.* (2004) found a much stronger correlation between foreshock area and the magnitude of the largest foreshock, instead of the magnitude of the mainshock, suggesting that foreshock area is not a useful predictor of the eventual mainshock size. Recent observations have found that foreshocks may be driven by an independent slow-slip phase (not part of the nucleation process), concurrently occurring within the fault zone (Kato

[1] University of Oklahoma, Norman, OK 73019, USA. E-mail: xiaowei.chen@ou.edu

[2] University of California, San Diego, La Jolla, CA 92093, USA.

Published online: 29 May 2015

*et al.* 2012; Chen and Shearer 2013), or within a wide region along the plate interface for interplate earthquakes (Bouchon *et al.* 2013).

The relative location and time between foreshocks and mainshocks is of great importance in recognizing foreshock sequences. For the foreshock sequences in Abercrombie and Mori (1996), all but one continue to the last day before the mainshock within 5 km of its hypocenter. In Bouchon *et al.* (2013), 70 % of interplate earthquakes have foreshocks continuous to the last day, but within a much larger spatial extent (up to 50 km). For the three M7 mainshocks in southern California, high-resolution earthquake catalogs reveal foreshock activities concentrated within hours of the mainshock Chen and Shearer (2013) within 0.5–2 km of the mainshock hypocenter. Some oceanic transform faults have enhanced immediate foreshock activities within hours before mainshocks within 5 km McGuire (2005). These observations suggest that, if foreshocks exist, they typically continue to immediately before the mainshock; thus, if a sequence is identified as a foreshock sequence, such as the 2014 Chile earthquake (Kato and Nakagawa 2014), the location and time of the eventual mainshock may be predicted.

Studies have found foreshock occurrence is dependent on the regional stress field, e.g., normal faulting versus reverse faulting Abercrombie and Mori (1996), or intraplate earthquakes versus interplate earthquakes (Bouchon *et al.* 2013), suggesting that the occurrence of foreshocks is not purely random, but may be influenced by the regional stress field. In this regard, retrospective searches of foreshock occurrence patterns in a variety of tectonic settings will be useful for future prospective forecasts.

Recently developed high-resolution catalogs provide opportunities to review previously identified foreshock features, and further probe the possible relationships among precursory seismicity, characteristics of earthquake clusters, and mainshock properties, which may be helpful in developing or improving earthquake forecasting models. In this study, we first retrospectively search for foreshocks for mainshocks ($M \geq 5$) and compare foreshock occurrence with mainshock faulting type, location, and foreshock and mainshock magnitudes, in order to see if there are any patterns in the apparent randomness of foreshock occurrence, and if there is any relationship between foreshock properties and mainshock parameters. We then investigate the occurrence patterns of small clusters that resemble swarm-like foreshock sequences but which do not always lead to larger events, and perform comparisons with synthetic catalogs based on an ETAS-like triggering model (epidemic-type-aftershock-sequence: a branching point process where the total seismicity rate is a summation of all triggered aftershocks from prior events, Ogata 1999), in order to examine to what extent the statistical model can explain the observed seismicity patterns.

## 2. *Foreshock Occurrence Pattern for $M \geq 5$ Earthquakes*

We search for isolated mainshocks with $M \geq 5$ using two waveform relocated catalogs in California (with relative location accuracy typically less than 200 m): (1) the Hauksson *et al.* (2012) catalog for southern California from 1981 to 2011, excluding events north of 35.5° and south of 32.0°; (2) the double-difference catalog for northern California from 1984 to 2009, excluding events south of 35.5° and north of 39.5° (data source: http://www.ldeo.columbia.edu/~felixw/NCAeqDD/) Waldhauser and Schaff (2008). The areas excluded are beyond the coverage of the regional network recording the events and thus likely have higher detection thresholds and larger location errors. To reduce potential catalog incompleteness issues for smaller earthquakes, we use events with $M \geq 1.5$ throughout this study. We select mainshocks that are relatively isolated from other large events, i.e., events that are not part of aftershock sequences or immediate foreshocks of larger events. Specifically, we exclude: (1) smaller events within 10 days and 50 km after $M \geq 5$ events; (2) smaller events within 120 days after $M \geq 6$ events; (3) smaller events immediately before a $M \geq 5$ event within 2 days and 5 km. These requirements are not an attempt to decluster the catalog, but rather to ensure the mainshocks that we analyze are largely independent from other large events (e.g., not within direct aftershock sequences or

when the catalog is temporarily influenced by the occurrence of a large event). Tests without applying such criteria resulted in several large "mainshocks" that are clear aftershocks of previous larger events (two are within the aftershock zone of a M6 earthquake and one is within a long-lasting swarm in the Long Valley volcanic region), in which their "foreshocks" cannot be distinguished from aftershocks of the earlier event. In total, 70 mainshocks in the two catalogs meet our criteria. Visual examination found five of these events are part of long-duration continuous sequences, and are excluded from the final list. The M6.6 event on the Superstition Hills fault in 1987 occurred 12 h following the M6.2 Elmore Ranch earthquake (noted with "*" in Table 1) and is excluded from the final list, because its precursory seismicity is dominated by seismicity following the first event.

Among the 64 mainshocks, 3 are within earthquake swarms in Nevada and the Salton Trough, and 3 are earthquake doublets (two events of similar magnitude occurring almost instantaneously, listed with "**" in Table 1). For the remaining 58 mainshocks, we examine the precursory activity within 50 km and 100 days before the mainchock. The scatter plot of days before the mainshock and distance to the mainshock suggests that most of the precursory activity is concentrated within 5 km of the mainshock hypocenters (Fig. 1). For most of the mainshocks that have precursory activity within 5 km, the cumulative number of foreshocks steadily grows until up to 30 days before the mainshocks, an increased rate of foreshocks occurs within approximately 20 days before, and significantly enhanced activity occurs within 2 days before the mainshocks (see Fig. 2). To check if the apparent acceleration behavior is dominated by a few larger sequences, we normalize event occurrence time by the duration of the precursory sequence (see Table 2 for calculation of duration), then calculate the cumulative density function (CDF) for each sequence, and average all sequences to get an averaged CDF for all mainshocks. Individual sequences have considerable scatter, however, the averaged CDF suggests enhanced precursory activities within the last 20 % of the total precursor duration (see Fig. 3), where the seismicity rate is significantly above the steady background rate.

Based on the broad spatial–temporal behavior of the precursory activities, we define foreshocks in this study as immediate precursory activity within 30 days and 5 km of the mainshock. Because foreshocks can only be identified in relation to their spatial and temporal proximity to mainshocks, there is no perfect method to separate foreshocks from 'background' activity, just as there is no way to uniquely discriminate very late aftershocks from background activity. We believe our 30-day and 5-km cutoff is a reasonable and practical choice (see scatter plot in Fig. 1) to ensure that the vast majority of our foreshocks are indeed foreshocks and not background activity. Using a larger spatial and/or temporal window might yield more foreshocks, but at the cost of including many background events. We use a fixed selection window regardless of mainshock magnitude to avoid biasing any comparisons between foreshock and mainshock properties.

We find that 27 of the 58 mainshocks (excluding the 3 swarms and 3 doublets) have no foreshocks within 30 days and 5 km. Among the 31 mainshocks with foreshocks, 14 mainshocks have "swarm-like" foreshocks (with more than 3 events, so we are able to estimate foreshock area in the following section, and the foreshocks do not start with the largest foreshock). Some special cases are included (noted with "*" in Table 1): (1) the 1986 Mt. Lewis sequence has a swarm with 14 events that occurred 7 days before the mainshock, which are included in the foreshocks; (2) for the 1986 Chalfant earthquake, a M5.9 event occurred 1 day before the M6.4 event, and the former is assumed to be the mainshock, with 40 foreshocks. Thus, from the 64 mainshocks examined here, excluding 3 swarms and 3 doublets, 53 % have at least one foreshock (58 % if including the swarms and doublets). A list of foreshocks is in Table 1 and a map view of the mainshock locations is shown in Fig. 4.

Our observed 53 % rate of foreshock occurrence is consistent with previous work. Abercrombie and Mori (1996) found a 44 % rate of $M \geq 2$ foreshocks prior to $M \geq 5$ events in the western United States. However, as noted by Reasenberg (1999), one expects the rate of foreshock occurrence to increase for lower foreshock magnitude cutoffs compared to the mainshock, so studies are best compared by dividing the

Table 1

*List of foreshocks with $M \geq 5$ included in this study*

| Time | Location | Depth | Mag | $N_{fore}$ | Focal mechanism | | Fault type | $Plane_{diff}$ |
|---|---|---|---|---|---|---|---|---|
| 1981/09/04 15:50:49.62 | 33.650°, −119.121° | 10.92 (5.00) | 5.45 | 0 | 134.77°, 169° | (311.90°, 180°) | 0.12 (0.00) | 12.94 |
| 1986/07/08 09:20:44.06 | 34.001°, −116.606° | 13.25 (10.00) | 5.65 | 0 | 298.38°, −177° | (294.37°, 156°) | −0.03 (0.27) | 3.33 |
| 1986/07/13 13:47:9.12[a] | 32.988°, −117.863°[a] | 21.36 (5.00)[a] | 5.45[a] | 0[a] | 359.72°, −167° | (126.37°, 106°)[a] | −0.14 (0.82)[a] | 43.86[a] |
| 1987/10/01 14:42:19.66 | 34.067°, −118.092° | 13.50 (11.00) | 5.90 | 0 | 262.23°, 83° | (270.31°, 98°) | 0.92 (0.91) | 10.71 |
| 1988/06/10 23:06:42.52 | 34.931°, −118.742° | 9.46 (N/A) | 5.37 | 0 | 162.83°, 176° | (N/A) | 0.04 (N/A) | N/A |
| 1988/12/03 11:38:26.26 | 34.142°, −118.138° | 12.74 (N/A) | 5.02 | 0 | 157.86°, 169° | (N/A) | 0.12 (N/A) | N/A |
| 1991/06/28 14:43:54.47 | 34.266°, −117.989° | 9.64 (11.00) | 5.80 | 0 | 56.25°, 74° | (93.43°, 130°) | 0.82 (0.56) | 35.15 |
| 1991/12/03 17:54:36.20 | 31.718°, −115.821° | 18.31 (N/A) | 5.32 | 0 | N/A | (N/A) | 0.00 (N/A) | N/A |
| 1993/05/28 04:47:40.26 | 35.132°, −119.116° | 23.90 (N/A) | 5.19 | 0 | 114.71°, 170° | (N/A) | O.11 (N/A) | N/A |
| 1994/01/17 12:30:54.96 | 34.206°, −118.549° | 21.07 (18.00) | 6.70 | 0 | 113.36°, 106° | (278.42°, 65°) | 0.82 (0.72) | 13.00 |
| 2001/12/08 23:36:10.03 | 32.035°, −114.963° | 17.23 (10.00) | 5.70 | 0 | N/A | (141.59°, −149°) | N/A (−0.34) | N/A |
| 2004/09/29 22:54:54.20 | 35.385°, −118.629° | 7.30 (3.50) | 5.03 | 0 | 105.82°, 173° | (293.71°, −169°) | 0.08 (−0.12) | 11.13 |
| 2008/02/09 07:12: 6.84 | 32.410°, −115.312° | 18.65 (2.90) | 5.10 | 0 | 147.66°, −175° | (226.79°, 3°) | −0.06 (0.03) | 24.25 |
| 2008/07/29 18:42:15.28 | 33.946°, −117.767° | 14.89 (14.70) | 5.39 | 0 | 296.66°, 146° | (44.55°, 29°) | 0.38 (0.32) | 34.85 |
| 2008/12/06 04:18:42.29 | 34.812°, −116.423° | 9.33 (7.30) | 5.06 | 0 | 172.79°, −157° | (253.83°, 6°) | −0.26 (0.07) | 12.02 |
| 1984/01/23 05:40:20.03 | 36.390°, −121.886° | 7.73 (N/A) | 5.10 | 0 | 65.85°, l0° | (N/A) | 0.11 (N/A) | N/A |
| 1984/04/24 21:15:18.75 | 37.310°, −121.682° | 7.97 (8.00) | 6.20 | 0 | 240.80°, 10° | (333.76°, 179°) | 0.11 (0.01) | 16.66 |
| 1988/02/20 08:39:57.49 | 36.798°, −121.306° | 8.22 (N/A) | 5.10 | 0 | 45.60°, 10° | (N/A) | 0.11 (N/A) | N/A |
| 1988/06/27 18:43:22.65 | 37.129°, −121.894° | 11.54 (N/A) | 5.30 | 0 | 35.85°, 30° | (N/A) | 0.33 (N/A) | N/A |
| 1988/09/19 02:56:31.33 | 38.458°, −118.344° | 6.72 (N/A) | 5.30 | 0 | 40.50°, −10° | (N/A) | −0.11 (N/A) | N/A |
| 1989/08/08 08:13:27.51 | 37.153°, −121.926° | 12.59 (N/A) | 5.40 | 0 | 45.65°, 30° | (N/A) | 0.33 (N/A) | N/A |
| 1989/10/18 00:04:15.39 | 37.043°, −121.877° | 16.41 (19.00) | 7.00 | 0 | 130.75°, 130° | (235.41°, 29°) | 0.56 (0.321) | 46.77 |
| 1991/09/17 21:10:29.35 | 35.815°, −121.322° | 8.01 (N/A) | 5.20 | 0 | 80.55°, 50° | (N/A) | 0.56 (N/A) | N/A |
| 1993/05/17 23:20:49:15[a] | 37.171°, −117.782°[a] | 2.39 (7.00)[a] | 6.40[a] | 0[a] | 250.65°, 20° | (210.30°, −93°)[a] | 0.22 (−0.97)[a] | 42.81[a] |
| 1996/11/27 20:17:23.54 | 36.090°, −117.628° | 6.56 (1.00) | 5.10 | 0 | N/A | (244.71°, −3°) | N/A (−0.03) | N/A |
| 2003/12/22 19:15:56.21 | 35.701°, −121.099° | 8.05 (7.60) | 6.50 | 0 | 105.35°, 80° | (296.32°, 88°) | 0.89 (0.98) | 9.73 |
| 2004/09/28 17:15:24.31 | 35.818°, −120.366° | 8.20 (8.80) | 6.00 | 0 | 145.85°, −170° | (321.72°, −178°) | −0.11 (−0.02) | 13.02 |
| 1988/12/16 05:53:4.48 | 33.983°, −116.688° | 11.47 (N/A) | 5.03 | 6 | 292.41°, 148° | (N/A) | 0.36 (N/A) | N/A |
| 1987/02/07 03:45:14.97[a] | 32.388°, −115.317°[a] | 24.44 (5.00)[a] | 5.38[a] | 2[a] | 235.87°, 98° | (202.70°, 2°)[a] | 0.91 (0.02)[a] | 17.55[a] |
| 1997/04/26 10:37:30.38 | 34.376°, −118.673° | 13.67 (N/A) | 5.07 | 1 | 358.52°, −141° | (N/A) | −0.43 (N/A) | N/A |
| 2001/10/31 07:56:16.22 | 33.504°, −116.503° | 16.83 (N/A) | 5.02 | 1 | 301.35°, 172° | (N/A) | 0.09 (N/A) | N/A |
| 2002/02/22 19:32:41.50 | 32.309°, −115.315° | 19.91 (7.00) | 5.70 | 2 | N/A | (190.66°, −4°) | N/A (−0.04) | N/A |
| 2005/06/12 15:41:46.19 | 33.533°, −116.570° | 15.48 (14.20) | 5.20 | 1 | 304.58°, 172° | (305.53°, −179°) | 0.09 (−0.01) | 5.03 |
| 2006/05/24 04:20:26.05 | 32.303°, −115.223° | 14.38 (N/A) | 5.37 | 2 | 0.0°, 0° | (N/A) | N/A (N/A) | N/A |
| 2009/09/19 22:55:17.64[a] | 32.344°, −115.256°[a] | 19.08 (3.00)[a] | 5.08[a] | 1[a] | 67.38°, 75° | (125.7°, −172°)[a] | 0.83 (−0.09) | 44.09[a] |
| 2009/12/30 18:48:56.69[a] | 32.417°, −115.149°[a] | 23.81 (9.00)[a] | 5.80[a] | 2[a] | 205.40°, −92° | (328.82°, −178°)[a] | −0.98 (−0.02) | 45.98[a] |
| 1984/11/23 18:08:25.25 | 37.455°, −118.606° | 11.11 (N/A) | 6.10 | 1 | 65.65°, 30° | (N/A) | 0.33 (N/A) | N/A |
| 1986/01/26 19:20:51.18 | 36.803°, −121.284° | 7.10 (7.00) | 5.50 | 1 | 260.80°, −110° | (166.90°, 180°) | −0.11 (0.00) | 9.97 |
| 1987/02/14 07:26:50.39[a] | 36.171°, −120.339°[a] | 13.55 (13.0)[a] | 5.30[a] | 1[a] | 150.50°, 90° | (300.46°, 38°)[a] | 1.00 (0.42)[a] | 20.24[a] |
| 1988/06/13 01:45:36.38 | 37.395°, −121.739° | 8.87 (9.00) | 5.30 | 1 | 60.90°, −10° | (325.76°, −175°) | −0.11 (0.06) | 13.97 |
| 1990/10/24 06:15:20.01 | 38.053°, −119.125° | 12.38 (12.00) | 5.80 | 1 | 70.55°, 10° | (56.59°, −10°) | 0.11 (−0.11) | 8.58 |
| 1996/01/07 14:32:52.82 | 35.772°, −117.622° | 9.56 (N/A) | 5.10 | 2 | 160.80°, −170° | (N/A) | −0.11 (N/A) | N/A |
| 2007/10/31 03:04:54.87 | 37.432°, −127.777° | 7.49 (10.00) | 5.40 | 1 | 55.85°, 0° | (324.81°, 176°) | 0.00 (0.04) | 10.18 |
| 1994/09/12 12:23:42.94 | 38.793°, −119.702° | 2.94 (14.00) | 5.90 | 1 | 40.40°, −40° | (42.74°, −13°) | −0.44 (−0.14) | 34.01 |
| 1987/11/24 01:54:14.21 | 33.082°, −115.779° | 10.07 (5.00) | 6.20 | 6* | 280.86°, 171° | (305.90°, 180°) | 0.10 (0.00) | 3.95 |
| 1990/02/28 23:43:36.23 | 34.138°, −117.708° | 7.28 (10.00) | 5.51 | 4 | 132.89°, 167° | (307.73°, 169°) | 0.14 (0.12) | 16.00 |
| 1992/04/23 04:50:22.73 | 33.968°, −116.313° | 13.71 (10.00) | 6.10 | 6 | 344.85°, 171° | (81.87°, −1°) | 0.10 (−0.01) | 5.47 |
| 1992/06/28 11:57:33.85 | 34.202°, −116.435° | 7.01 (5.00) | 7.30 | 27 | 173.85°, −177° | (341.70°, −172°) | −0.03 (−0.09) | 15.14 |
| 1992/11/27 16:00:57.39 | 34.337°, −116.892° | 0.00 (N/A) | 5.29 | 5 | 128.88°, 167° | (N/A) | 0.14 (N/A) | N/A |
| 1997/03/18 15:24:47.70 | 34.966°, −116.822° | 4.02 (N/A) | 5.26 | 3 | 154.75°, −163° | (N/A) | −0.19 (N/A) | N/A |
| 1999/10/16 09:46:43.95 | 34.595°, −116.271° | 9.06 (0.00) | 7.10 | 18 | 5.90°, 159° | (336.80°, 174°) | 0.23 (0.07) | 9.95 |
| 2010/04/04 22:40:42.16 | 32.264°, −115.295° | 16.47 (6.00) | 7.20 | 26 | 264.49°, 165° | (223.84°, −2°) | 0.17 (−0.02) | 36.64 |
| 1985/08/04 12:01:55.85[a] | 36.138°, −120.153°[a] | 10.35 (5.00)[a] | 5.60[a] | 6[a] | 70.20°, 40° | (138.10°, 105°)[a] | 0.44 (0.83)[a] | 66.04[a] |
| 1986/03/31 11:55:39.93 | 37.479°, −121.691° | 8.39 (6.00) | 5.70 | 15* | 355.80°, −180° | (353.79°, −170°) | 0.00 (−0.11) | 1.06 |
| 1986/07/20 14:29:45.47 | 37.567°, −118.437° | 6.16 (8.00) | 5.90 | 40* | 205.85°, −10° | (223.54°, −35°) | −0.11 (−0.39) | 31.28 |
| 1990/04/18/ 13:53:51.62 | 36.931°, −121.652° | 4.61 (N/A) | 5.40 | 4 | 55.80°, 40° | (N/A) | 0.44 (N/A) | N/A |
| 1997/11/02 08:51:52.83 | 37.863°, −118.190° | 1.65 (5.00) | 5.30 | 8 | N/A | (238.63°, 15°) | N/A (0.17) | N/A |

Table 1

*continued*

| Time | Location | Depth | Mag | $N_{fore}$ | Focal mechanism | | Fault type | $Plane_{diff}$ |
|---|---|---|---|---|---|---|---|---|
| 1998/08/12 14:10:25.15 | 36.759°, −121.452° | 7.75 (8.80) | 5.10 | 3 | 225.75°, −10° | (48.85°, −1°) | −0.11 (−0.01) | 10.01 |
| 1981/04/26 12:09:28.26 | 33.088°, −115.619° | 10.60 (6.00) | 5.75 | 349 | 158.86°, −151° | (249.45°, −8°) | −0.32 (−0.09) | 45.03 |
| 2005/09/02 01:27:19.46[a] | 33.154°, −115.633°[a] | 5.77 (9.80)[a] | 5.11[a] | 387[a] | 190.62°, −106° | (335.76°, −167°)[a] | −0.82 (−0.14)[a] | 18.21[a] |
| 2008/04/26 06:40:10.76 | 39.522°, −119.927° | 2.28 (1.40) | 5.10 | 214 | N/A | (328.86°, 180°) | N/A (0.00) | N/A |
| 2001/07/17 12:07:26.24 | 36.005°, −117.871° | 8.73 (N/A) | 5.20 | 41** | 80.90°, 0° | (N/A) | 0.00 (N/A) | N/A |
| 2004/09/18 23:02:17.72 | 38.012°, −118.691° | 3.26 (5.00) | 5.60 | 42** | 65.90°, −10° | (330.76°, −171°) | −0.11 (−0.10) | 13.97 |
| 2009/10/03 01:15:59.75 | 36.396°, −117.858° | 0.29 (2.50) | 5.10 | 52** | N/A | (214.56°, −36°) | N/A (−0.40) | N/A |

CMT solutions are in parentheses

Events with "*" are special cases and events with "**" indicate earthquake doublets (see text for details)

[a] Events with a high degree of disagreement between CMT solutions and the regional moment tensor catalog

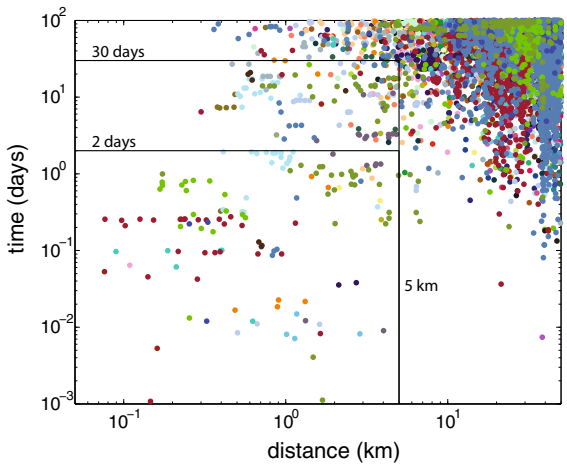


Figure 1
Scatter plot of all events within 50 km and 100 days before each mainshock (excludes the 3 swarms and 3 doublets). *Dots with the same color* belong to the same foreshock–mainshock sequence

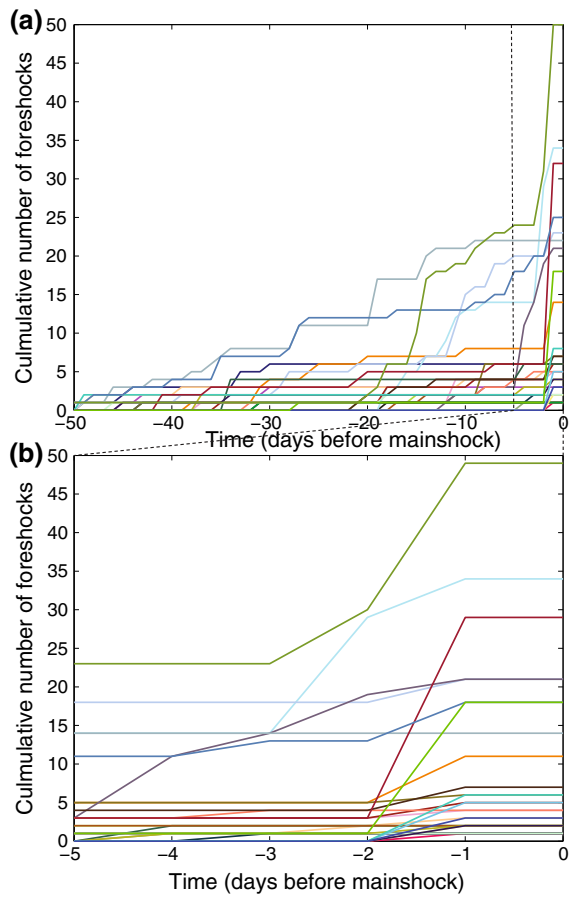


Figure 2
**a** Cumulative number of foreshocks within 5 km before each mainshock. *Vertical dashed line* marks 5 days before mainshock. **b** Closeup of the last 5 days before the mainshocks. The *colors* correspond to individual mainshock sequences in Fig. 1

apparent foreshock rate by the differential magnitude. In our case, we obtain a foreshock rate density of 15 % per magnitude unit. For comparison, Abercrombie and Mori (1996) obtained 15 % per magnitude unit, and Reasenberg (1999) obtained 13 % per magnitude unit from a global study of $M \geq 6$ events.

### 2.1. *Relationship Between Foreshock Properties and Mainshock Parameters*

Next, we examine if there is any relationship between foreshock properties and mainshock source

Table 2

*Definition of parameters, the superscript letter a are parameters analyzed in this study*

| | |
|---|---|
| $T_i$ | Time of each event |
| $T_0$ | Time of the first event |
| $X_i$ | 3D locations of each event |
| $M_0(i)$ | $10^{1.5*M(i)+9.1}$ |
| $t_i$ | $(T_i - T_0)/\text{mean}(T_i - T_0, i = 1...N)$ |
| $\bar{t}$ | $\sum_i^N t_i M_0(i) / \sum_i^N M_0(i)$ |
| $\mu_3$ | $\sum_i^N (t_i - \bar{t})^3 M_0(i)$ |
| $\delta$ | $\sqrt{\sum_i^N (t_i - \bar{t})^2 m_0(i)}$ |
| $C_i^j$ | Centroid location= median$(X_k, k = i..j)$ |
| $r^a$ | Radius = median$(\lvert X_i - C_1^N \rvert, i = 1...N)^a$ |
| $t_{\text{dura}}{}^a$ | Duration = median$(\lvert T_i - T_0 \rvert, i = 1...N)^a$ |
| $t_{\text{max}}{}^a$ | $t_i, \{M(i) = \max(M)\}^a$ |
| $\mu^a$ | $\mu_3/\delta^a$ |
| $\Delta\sigma_{\text{quasi}}{}^a$ | $\frac{7\sum_i^N M_0(i)_a}{16r^3}$ |
| $d_s{}^a$ | $(\lvert C_1^{N/2} - C_{N/2}^N \rvert)/r^a$ |
| $M_{f_{\text{max}}}{}^a$ | Maximum magnitude of foreshocks[a] |
| $N_{\text{fore}}{}^a$ | Number of foreshocks[a] |
| $M_{\text{max}}{}^a$ | Magnitude of mainshock[a] |
| $F_{\text{area}}{}^a$ | Area of foreshocks[a] |
| Swarm-type[a] | $t_{\text{max}} \geq 0.2^a$ |
| Aftershock-type[a] | $t_{\text{max}} < 0.2^a$ |

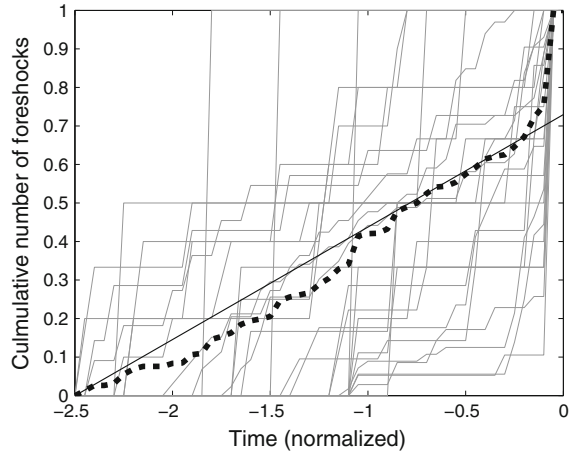


Figure 3
Cumulative density functions (CDF) with origin time normalized by duration of each precursory period, (see text and Table 2 for details). *Each grey line* corresponds to a individual mainshock, the *thin black line* is an approximation of a constant background rate. The *black dashed line* is the averaged CDF of all the *individual grey lines*, note the clear deviation from the constant rate within the last 20 % of the precursory period

parameters. We first compare foreshock occurrence with focal mechanism. We obtain focal mechanism solutions from: (1) the YHS (by YANG, HAUKSSON and SHEARER 2012) catalog for southern California, recalculated using the HASH method (in HARDEBECK and SHEARER 2003) with data from the Southern California earthquake center (YANG *et al.* 2012); (2) the northern California moment tensor catalog [*Northern California Earthquake Catalog and Phase Data*]; and (3) Global Centroid-Moment-Tensor (CMT) solutions when available. We compute faulting type based on rake angle ($-1$ is normal fault, 0 is strike–slip fault, 1 is reverse fault):

$$f = \begin{cases} \lambda/90 & \text{if } |\lambda| \leq 90; \\ (180 - |\lambda|) * (\lambda/|\lambda|)/90 & \text{if } |\lambda| > 90. \end{cases} \quad (1)$$

For 8 mainshocks, there is a high degree of mismatch ($>40°$ between fault plane orientations and $df = |f_{\text{regional}} - f_{\text{cmt}}| > 0.4$ between the global CMT solution and the regional network solution (see Table 1; Fig. 4). The mismatch may be due to reduced azimuthal station coverage for events outside the regional network (e.g., events off-shore and events in Mexico), or complexity in the earthquake rupture process (e.g., the rupture initiated with a sub-event with a different focal mechanism). Because the regional networks do not provide unique solutions for many events, we use CMT solutions when available.

We first examine foreshock occurrence in 10 faulting type bins from $-1$ to 1. From Fig. 5, there is a higher foreshock occurrence rate for mainshocks with dilational components ($f < 0$) and reverse-faulting mainshocks tend to have lower foreshock occurrence rates. Although some mainshocks have a larger degree of mismatch between the regional and CMT solutions, these events do not affect the overall trend of decreasing foreshock occurrence for reverse-faulting events. There is only one pure normal-faulting mainshock, which has no foreshock. However, with the regional focal mechanism catalog, all the normal-faulting earthquakes are preceded by at least one foreshock. Our result is most reliable for faulting types from $-0.4$ to 0.5, where an increase in the compressional component decreases foreshock occurrence for strike–slip faults. We also compare foreshock occurrence with mainshock depth from the two regional catalogs. In Fig. 5, for shallower events (mostly $\leq 5$ km), the majority of mainshocks have

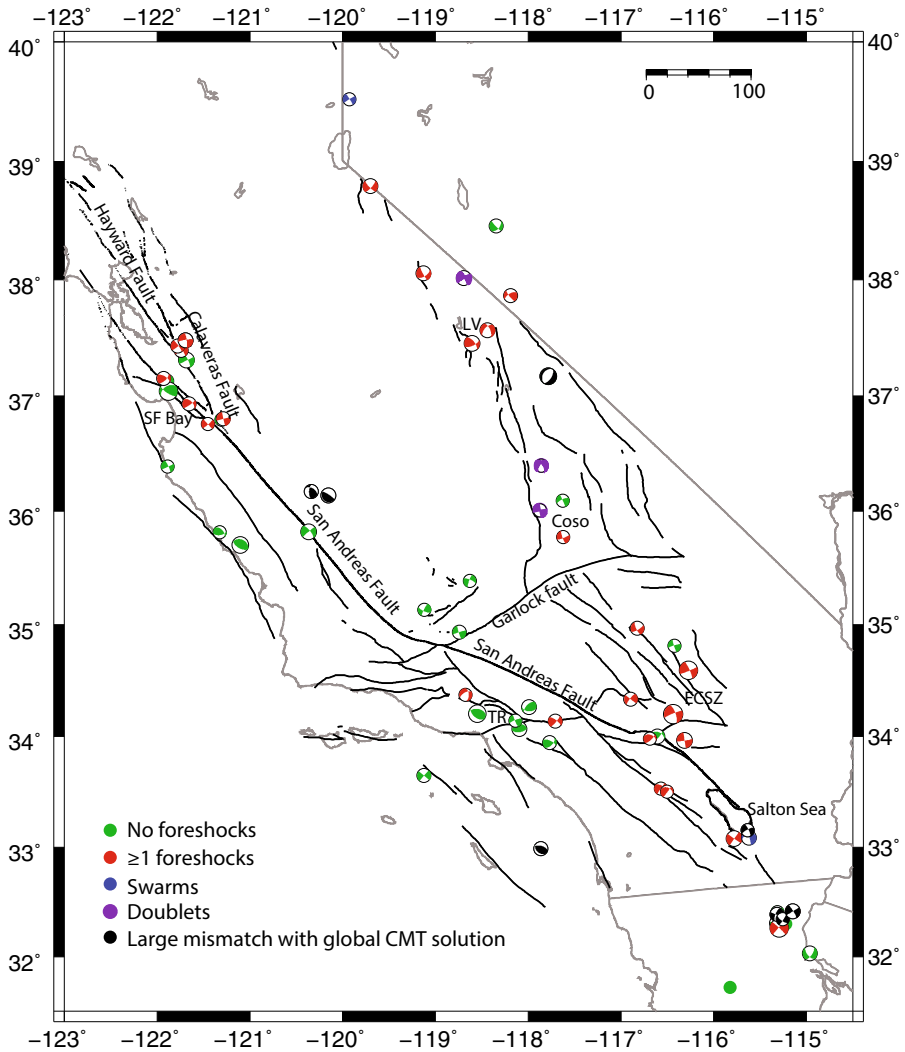


Figure 4
Map view of $M \geq 5$ mainshocks. Events with a large mismatch with CMT solutions correspond to events with red colors in Table 1). Focal mechanisms are from CMT solutions when available. Regions in the map: *TR* Transverse Range, *LV* Long Valley

foreshocks, and the occurrence rate decreases with depth. We test the statistical significance of the pattern with the Student's $t$ test (Abercrombie and Mori 1996). For this, we divide foreshock occurrence rate into several groups in faulting type and depth: for faulting type, we use −0.5–0 ($f1$), 0–0.5 ($f2$), and 0.5–1 ($f3$); for depth, we use 0–5 and 5–25 km. For faulting type, group $f1$ is different from $f2$ and $f3$ at a 97 % confidence level, while $f2$ and $f3$ are similar; for depth, the shallow group is different from the deeper group at a 98 % confidence level. We also examine the relationship between faulting type and depth (see Fig. 6). The shallowest events spread evenly between $f = -0.5$ and $f = 0.5$. For events deeper than 5 km, there is no clear dependence between faulting type and depth, and a faulting type dependence of foreshock occurrence is clear. Thus, the most reliable trends are a dependence on faulting type for $-0.5 \leq f \leq 1$ and a higher foreshock occurrence rate at shallow depth.

We compare foreshock properties with mainshock magnitude by examining: (1) the radius of foreshock rupture area for the 14 swarm-like foreshock sequences; (2) the number of foreshocks; (3) the magnitude of the largest foreshock; and (4) foreshock duration (see Table 2 for definitions). For the three

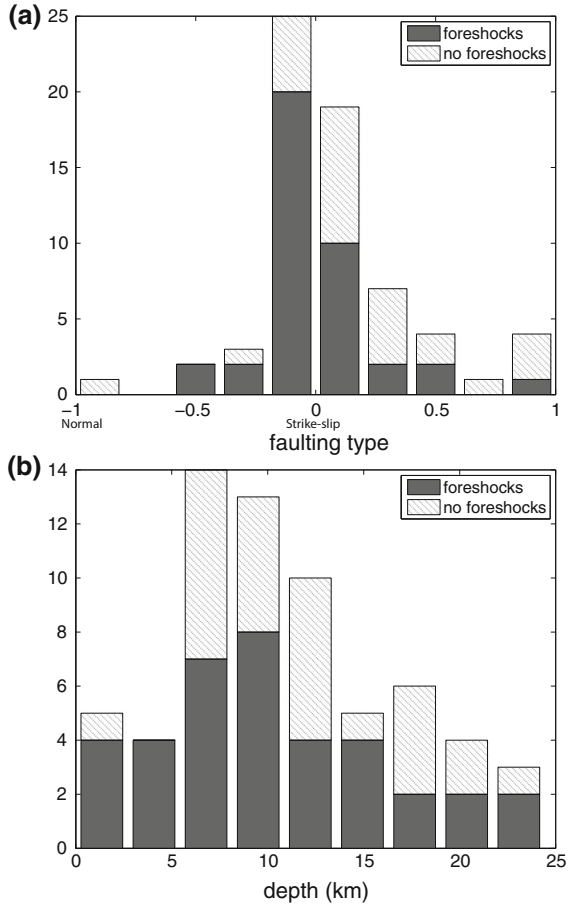


Figure 5
**a** Histogram of faulting types for 27 mainshocks without foreshocks and 37 mainshocks with foreshocks. Faulting types from −1 to 0 to 1 correspond to normal faulting–strike slip–reverse faulting, respectively. **b** Histogram of the depth distribution for 27 mainshocks without foreshocks and 37 mainshocks with foreshocks. Note the prevalence of foreshock occurrence at shallow depth and for transtentional faults ($f \leq 0$, for definition of $f$, refer to Eq. 1). We perform a Student's $t$ test to examine the statistical significance of the pattern (Abercrombie and Mori 1996). For faulting types, the group of −0.5 to 0 is different from 0 to 1 at 97 % confident level, and the shallow group ($\leq 5$) is different from the rest at 98 % confident level

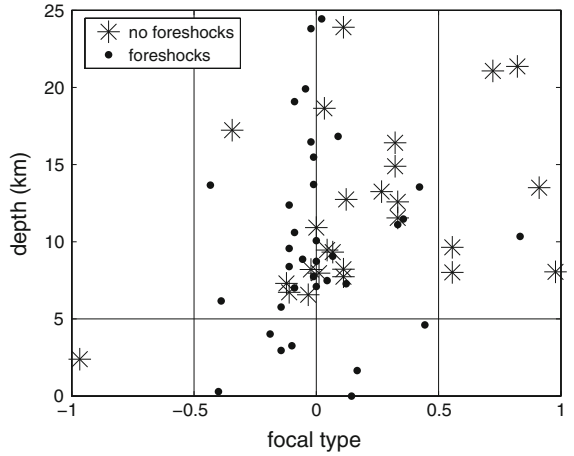


Figure 6
Scatter plot of depth versus faulting type for each mainshock. *Black dots* are mainshocks with foreshocks, *black stars* are mainshocks without foreshocks. The *vertical lines* corresponds to the three groups that we test against for faulting types. The *horizontal line* marks the depth groups that we test against. For events deeper than 5 km, there is no clear relationship between faulting type and depth, and the most prominent feature is a faulting type dependence of foreshock occurrence

$M > 7$ mainshocks (the 1992 Landers, the 1999 Hector Mine and the 2010 El Mayor-Cucapah earthquakes), we have shown that none of these properties are correlated with mainshock magnitude (Chen and Shearer 2013). For each of the 14 mainshocks, we visually check seismicity within each mainshock rupture zone using an interactive tool, to ensure a good selection of foreshocks from the automatic search process described above. We also compare two different methods to estimate foreshock area, specifically: (1) we calculate area based on the radius assuming a circular area; (2) we compute the convex polygon that includes all foreshocks. Both methods yield similar results, where mainshock magnitude is correlated with the number of foreshocks, but not foreshock area, while foreshock area is correlated with the number of foreshocks and the magnitude of the largest foreshock (see Table 3). The lack of correlation of foreshock area with mainshock magnitude, but with foreshock number and magnitude, suggests foreshock processes are controlled by interactions within foreshocks themselves, rather than being an indicator of mainshock magnitude. Most of the foreshocks do not start with their largest event, suggesting the "swarmy" nature of foreshock sequences. The fact that mainshock magnitude is correlated with the number of foreshocks suggests that swarms with many events increase the probability of large earthquakes, such as the 1975 Haicheng sequence, the 1992 Landers and the 1999 Hector Mine earthquakes.

Overall, observations of foreshock dependence on faulting type and depth are consistent with the results in Abercrombie and Mori (1996); however, our result

Table 3

*Correlation between foreshock properties and mainshock parameters*

| | |
|---|---|
| $M_{\max} - F_{\text{area}}$ (convex) | $cc = 0.46, p = 0.11$ |
| $M_{\max} - F_{\text{area}}$ (radius) | $cc = 0.32, p = 0.28$ |
| $M_{\max} - N_{\text{fore}}$ [a] | $cc = 0.62, p = 0.02$[a] |
| $M_{\max} - M_{f\max}$ | $cc = 0.07, p = 0.86$ |
| $M_{\max} - t_{\text{dura}}$ | $cc = 0.10, p = 0.75$ |
| $M_{f\max} - F_{\text{area}}$ (convex)[a] | $cc = 0.56, p = 0.05$[a] |
| $M_{f\max} - F_{\text{area}}$ (radius)[a] | $cc = 0.60, p = 0.03$[a] |
| $N_{\text{fore}} - M_{f\max}$ | $cc = 0.11, p = 0.73$ |
| $N_{\text{fore}} - F_{\text{area}}$ (convex)[a] | $cc = 0.69, p = 0.01$[a] |
| $N_{\text{fore}} - F_{\text{area}}$ (radius)[a] | $cc = 0.58, p = 0.04$[a] |

($cc$ is correlation coefficient, and $p$ is the statistical significance of correlation, $p \leq 0.05$ is generally considered as significantly above random chance)

[a] Significant correlation

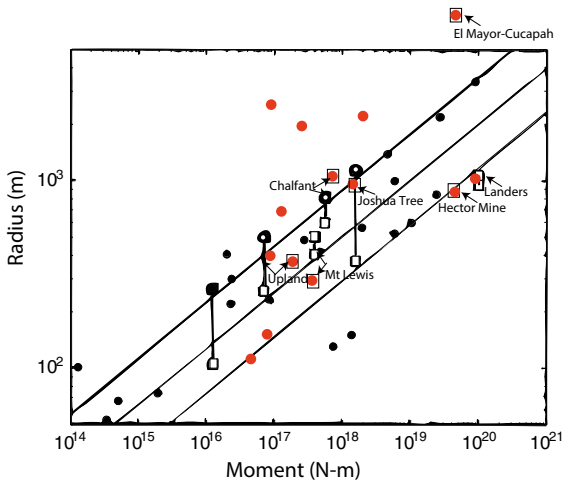


Figure 7

Foreshock radius versus mainshock moment plotted on Figure 16 from Dodge *et al.* (1996). *Red dots* are 14 mainshocks in this study, *boxes* indicate named events in the catalog. *Black dots* are source radii estimated in Beroza and Ellsworth (1996), *straight lines* are best-linear fit and $1\sigma$ boundaries. Note the scattered *red dots* above the $1\sigma$ limit. The $p$ value of the correlation for the *red dots* is 0.28, indicating no statistical significance (see Table 3)

is more reliable for strike–slip faults and shallow depths, because we have used improved catalogs, examined more events and obtain consistent results with both regional and CMT catalogs. It is interesting to compare our foreshock radius estimates with results in Dodge *et al.* (1996) (see Fig. 7). In general, for the events in common, our radius is consistent with previous measurements; however, about half of the points are above the $1\sigma$ boundaries of nucleation radius estimated from the slow onset of mainshock waveforms (Ellsworth and Beroza 1995). There is no correlation between foreshock duration and mainshock depth ($cc = 0.15, p = 0.62$), which is inconsistent with previous observations (Jones 1984; Abercrombie and Mori 1996). There is some degree of spatial separation between different types of mainshocks: within the Transverse Range region in Los Angeles county and central California, most mainshocks do not have foreshocks; in contrast, in the San Francisco Bay area and Eastern California Shear Zone (ECSZ), at the intersection of different faults, the occurrence rate of foreshocks is relatively high (see Fig. 4).

### 2.2. *Precursory Seismicity*

The rupture area of a M5.8 earthquake is about 5 km, assuming a stress drop of 2 MPa (the average stress drop for southern California from Shearer *et al.* (2006), calculated from Shearer (2009), with $r = \left(\frac{7M_0}{16\Delta\sigma}\right)^{1/3}$. According to Shearer and Lin (2009), the radius of the "Mogi-doughnut" (enhanced precursory seismicity) roughly agrees with the expected rupture radius for target mainshocks. Due to the small number of M5 earthquakes in the catalog, such behavior is not reliably resolved for larger events in their study. For the 64 M $\geq$ 5 mainshocks, we examine the averaged precursory seismicity for: (1) 27 mainshocks without foreshocks; (2) 31 mainshocks with foreshocks; (3) 3 earthquake swarms; and (4) 3 earthquake doublets. For each group, we calculate seismicity density for each time and distance bin based on: $D = \frac{n}{N(t_2 - t_1)(4/3)\pi(r_2^3 - r_1^3)}$, where $n$ is the total number of precursory events in the space/time bin, and $N$ is the number of target events in each group. We use 100 space-time bins, evenly spaced in 10 log distance bins between 0.01 and 100 km, and in 10 log time bins from 0.001 to 1000 days. From Fig. 8, within 1 day prior to the mainshock, the low seismicity zone extends beyond the 5 km criteria, consistent with the empirical scaling of "Mogi doughnut" behavior. Due to the limited number of available mainshocks, we do not attempt to perform statistical analysis to test the reliability of the "Mogi" zone relative to smaller event bins from Shearer and Lin (2009). Foreshock activity is confined within the "Mogi" zone, and well

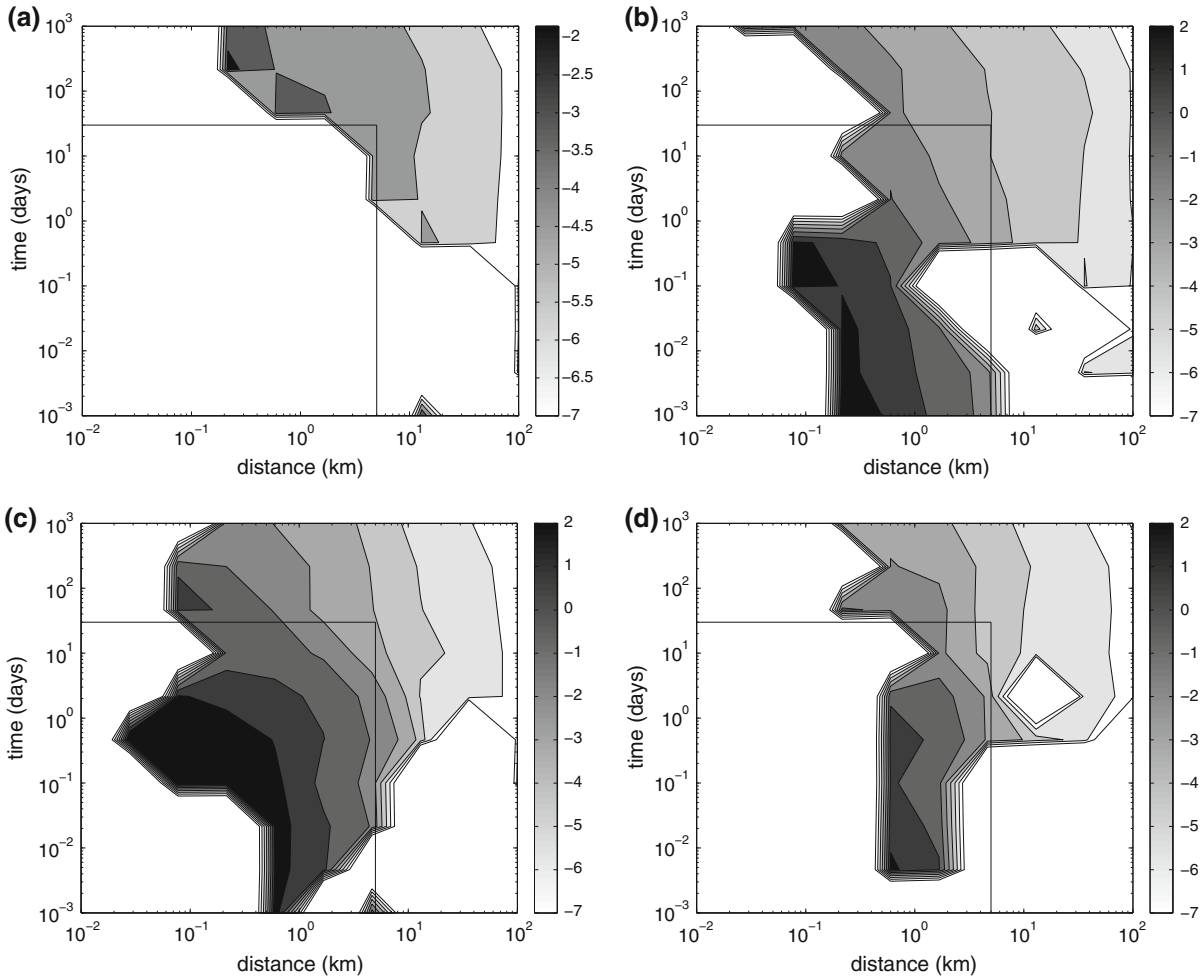


Figure 8
Precursory seismicity within 1000 days and 100 km prior to target mainshocks with $M > 5$. Four mainshock types are included: **a** mainshocks with no foreshocks; **b** mainshocks with $\geq 1$ foreshocks; **c** earthquake swarms; **d** earthquake doublets. *Horizontal black lines* correspond to $T = 2$ days, *vertical black lines* correspond to $D = 5$ km. The *color scale* shows $\log_{10}$ of seismicity rate in each distance-time bin

separated from background seismicity. The high event density per time/distance bin suggests that foreshocks are highly localized within future mainshock rupture zones (also see Fig. 1).

## 3. Seismicity Clusters that Resemble Foreshock Sequences

So far, our analysis has been limited to $M \geq 5$ target events, and any foreshock activities within 5 km and 30 days. However, there are other important questions related to precursory activities, such as: (1) how are foreshock sequences different from random small clusters? (2) How often do small clusters lead to larger clusters that might include a larger event? To address this, we remove the magnitude requirement, and search for small compact clusters that resemble the observed foreshock sequences. Specifically, we search for small clusters that have at least $N \geq 10$ events within 5 km and 2 days, and fewer than 5 events in the previous 7 days within 5 km. The 2-day requirement is based on the observation that enhanced activities typically occur within 2 days before mainshocks (see Fig. 2), the number requirement is to ensure the relative independence of

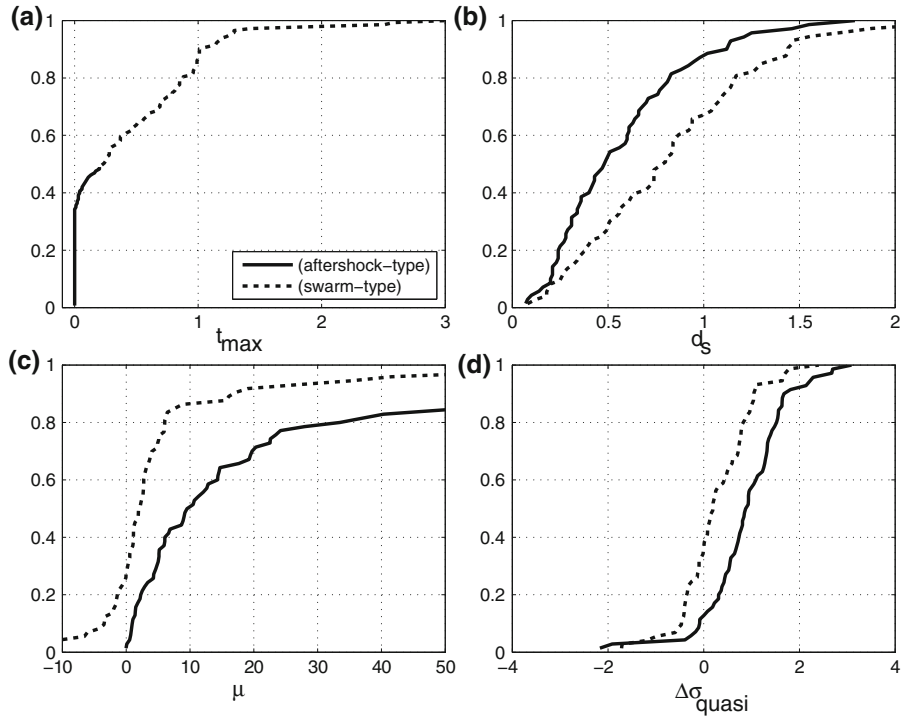


Figure 9
Distribution of different parameters for: "aftershock-type" ($t_{\max} \leq 0.2$) (*solid line*) and "swarm-type" ($t_{\max} \geq 0.2$) (*dashed line*) sequences from combined observations in southern and northern California. **a–d** Correspond to the four parameters discussed in the text: $t_{\max}$, $d_s$, $\mu$, $\Delta\sigma_{\text{quasi}}$

the small cluster, and minimize the number of random scattered clusters. We apply the same criteria as before to temporarily remove immediate aftershock sequences from the catalog for consistency.

Next, we check whether these clusters grow into larger clusters. To define a larger cluster, we require: (1) $N_{\text{cluster}} \geq 50$ within 28 days and 5 km following the small cluster; (2) $N_{\text{outside}} \leq 0.2N_{\text{cluster}}$ within 28 days between 5 and 10 km. The latter requirement is to ensure the cluster is spatially isolated from background seismicity; however, it does not affect the relative distribution of different types of clusters. To characterize the cluster type, we compute four parameters as described in Chen *et al.* (2012) and listed in Table 2: (1) $t_{\max}$, the relative timing of the largest event in the cluster with respect to the mean delay time; (2) the skew ($\mu$) of moment release history; (3) the distance separation of the first and second half of the cluster normalized by the radius of the cluster ($d_s$); and (4) $\Delta\sigma_{\text{quasi}} = \frac{7\sum_n^1 M_0^i}{16r^3}$, the effective stress drop. The parameter $d_s$ is a proxy to measure the spatial migration of seismicity clusters, and $\Delta\sigma_{\text{quasi}}$ is a parameter to measure the effectiveness of moment release compared with the rupture area. The observations in Chen *et al.* (2012) suggested clusters with $t_{\max} \geq 0.2$ are more prone to spatial migration controlled by external aseismic transients. We use this empirical relationship, and define aftershock-type clusters as those with $t_{\max} \leq 0.2$, and swarm-type clusters as those with $t_{\max} \geq 0.2$. Foreshocks are any earthquakes occurring before the largest earthquake (mainshock) in the cluster, and all swarm-type clusters have foreshocks by definition.

For the southern California catalog, we identify 311 small clusters, of which 87 grow into larger clusters, and 27 start with their mainshock. Small clusters are less common in northern California, where we identify 184 small clusters, 56 of which grow into larger clusters, and 21 start with their mainshock. From Fig. 9, the CDF of the four parameters are consistent with Chen *et al.* (2012):

aftershock-type clusters have lower $d_s$, higher $\mu$ and higher $\Delta\sigma_{\text{quasi}}$.

Overall, in total 495 small clusters are identified, of which 30 % eventually grow into a larger cluster. Among the larger clusters, 66 % have precursory activities. If we only focus on aftershock-type larger clusters (see Table 2), there are 39 % with precursory activities. For southern California, we observe a similar relationship to $M \geq 5$ mainshocks between precursory occurrence and small mainshock faulting type (foreshock occurrence rate is higher for faulting-type $<0$), which is consistent with CHEN *et al.* (2012), however, the correlation is not so clear for northern California. For smaller events, the focal mechanism is likely poorly determined compared with $M \geq 5$ events, and the reduced correlation may be due to uncertainties in the fault plane solutions (as shown in Table 1, there is sometimes a large mismatch for $M \geq 5$ events). The southern California YHS catalog is improved compared to the routine catalog solutions, and likely is more accurate (YANG *et al.* 2012). For both catalogs, we observe a prevalence of precursory activities at shallow depth and a lack of precursory activities at deeper depth (Fig. 10).

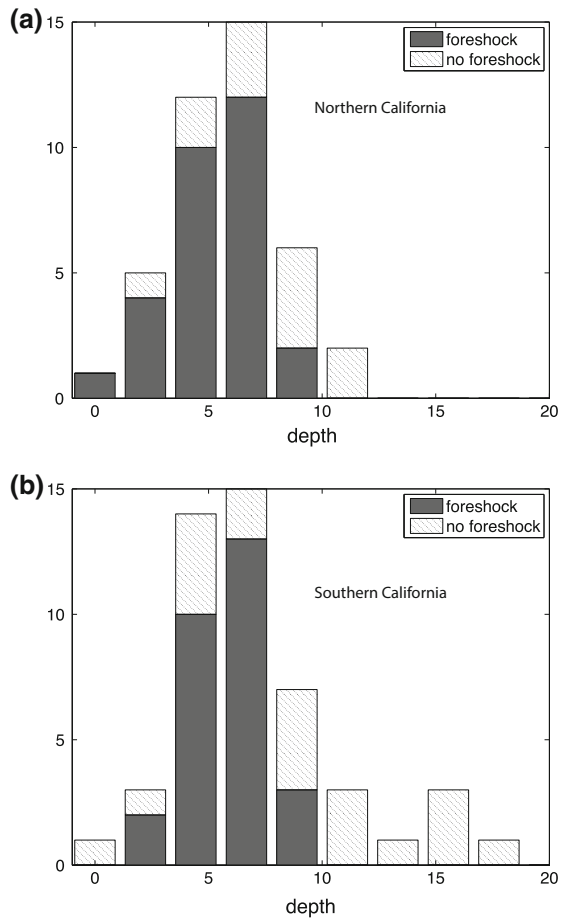


Figure 10
Depth distribution of all clusters with at least one foreshock and without foreshocks. **a** Northern California, **b** Southern California. The majority of mainshocks shallower than 8 have foreshocks, while all mainshocks deeper than 10 km have no foreshocks

The overall spatial distribution is similar for $M \geq 5$ mainshocks (see Figs. 4, 11). For example, the Transverse Ranges and central California are still dominated by mainshocks without foreshocks. The Bay Area, the ECSZ, the Salton Trough and the Long Valley region are dominated by mainshocks with foreshocks. Considering the geological features of these regions, this suggests that foreshocks tend to occur within extensional step overs, high heat flow regions, and complex fault zones, while a lack of foreshocks is expected at thrust fault zones and relatively simple planar fault zones. The consistency between foreshocks for $M \geq 5$ mainshocks and general clustering types suggests that localized fault zone properties control precursory activities.

We next investigate whether foreshock properties are predictive of mainshock parameters. We find that:

1. Neither foreshock area nor the number of foreshocks is correlated with mainshock magnitude; none of the other foreshock properties correlate with mainshock parameters.
2. Foreshock area is well correlated with the number of foreshocks: correlation coefficient $(cc) = 0.8, p = 10^{-5}$ (see Table 4).
3. If we consider swarms ($t_{\max} \geq 0.2$) as foreshock–mainshock sequences, then for clusters with $M_{\max} \geq 4.5$, foreshock area is correlated with the maximum magnitude of foreshocks ($M_{f\max}$) with $cc = 0.55, p = 0.005$, however, for clusters with $2 \leq M_{\max} \leq 4.5$, there is no correlation between foreshock area and $M_{f\max}$ (see Table 4).
4. The magnitude difference ($d_m$) between $M_{\max}$ and $M_{f\max}$ is dependent on $M_{\max}$: for $M_{\max} \geq 4.5$, $d_m$ is approximately uniformly distributed between 0.5 and 2, and the median value is 1.47; for $2 \leq M_{\max} \leq 4.5$, $d_m$ is skewed towards lower values, and is mostly below 1 (Fig. 12).

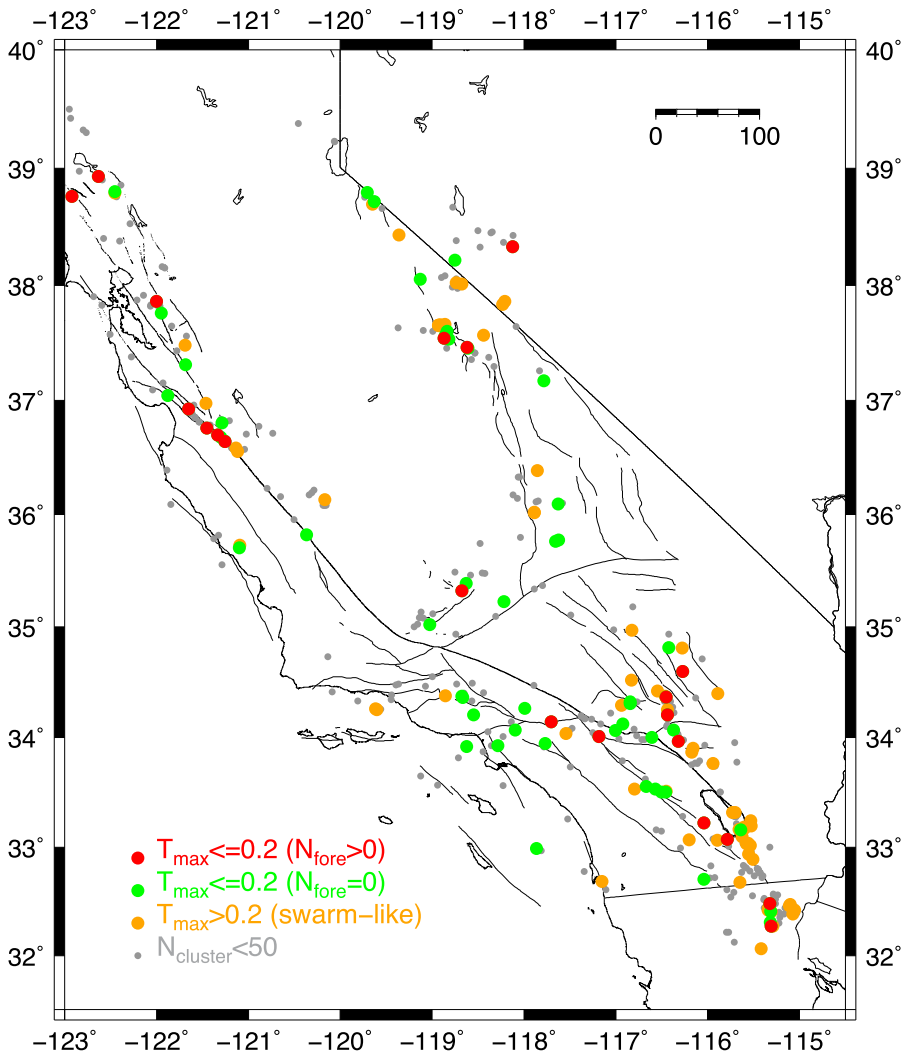


Figure 11
Map view of seismicity bursts in California. *Red dots* aftershock-type clusters with at least one foreshocks; *green dots* aftershock-type clusters without any foreshocks; *orange dots* swarm-type clusters (have foreshocks by definition); *grey dots* small random clusters that do not grow into large clusters

Table 4

*Correlation between foreshock area $F_{\text{area}}$, mainshock magnitude $M_{\max}$, magnitude of largest foreshock $M_{f\max}$ and number of foreshocks ($N_{\text{fore}}$) from combined result of southern and northern California*

| Type | $2 \le M_{\max} \le 4.5$ | $M_{\max} \ge 4.5$ |
|---|---|---|
| $F_{\text{area}}$ and $M_{\max}$ | $cc = 0.19, p = 0.15$ | $cc = 0.17, p = 0.43$ |
| $F_{\text{area}}$ and $M_{f\max}$ | $cc = 0.23, p = 0.083$ | $cc = 0.55, p = 0.005$ |
| $F_{\text{area}}$ and $N_{\text{fore}}$ | $cc = 0.74, p = 2.9e-11$ | $cc = 0.81, p = 1.4e-6$ |

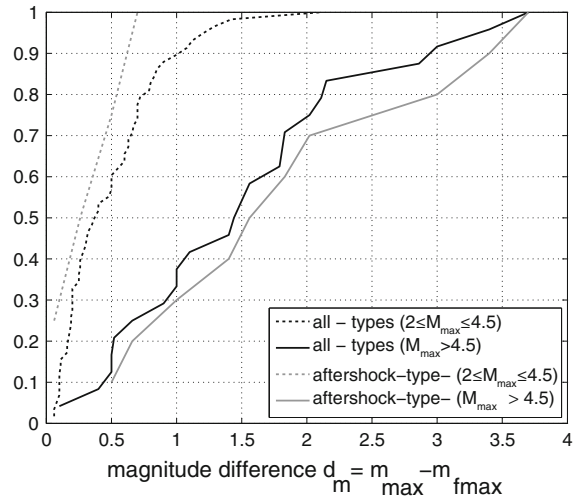


Figure 12
Magnitude difference between the mainshocks and their largest foreshock for combined observations from southern California and northern California. *Black lines* are for all cluster types (include both aftershock-type and swarm-type), *grey lines* only include aftershock-type clusters. *Dash lines* $2 \le M_{\max} \le 4.5$, *solid lines* $M_{\max} \ge 4.5$

Overall, results in this section confirm the relationship between foreshock parameters and $M \ge 5$ mainshocks in the previous section. However, we also find that the correlation between foreshock area and foreshock magnitude, and the magnitude difference distribution, are different for clusters with $2 \le M_{\max} \le 4.5$ and $M_{\max} \ge 4.5$, which may suggest different triggering processes for different sized earthquakes. Next, we examine whether or not these observations are consistent with synthetic catalogs generated based on empirical statistical relationships.

## 4. Comparison with Synthetic Catalogs

Earthquake-to-earthquake triggering models relate the probability of earthquakes to the past history of nearby earthquakes using Omori's law for aftershocks and other empirical relationships and have been extensively described by a number of authors (e.g., OGATA1999; HELMSTETTER *et al.* 2003, 2005; FELZER *et al.* 2004). To investigate which features of our observations are consistent with triggering models, we create synthetic catalogs based on the self-similar triggering model described by SHEARER (2012a) that is similar to the ETAS model (epidemic-type-aftershock-sequence) (OGATA 1999). In the models, each "parent" event independently triggers its own aftershock chain of "daughter" events. The number of direct aftershocks $N_{\text{asl}}$ for an event with magnitude $m$ follows a productivity law, and event probabliity follows a power-law decay in with time and distance:

$$\begin{aligned} N_{asl} &= Q10^{\alpha(m-m_1)} \\ N(r,t) &= N_{asl}(t+c)^{-p} r^{-q}, \end{aligned} \tag{2}$$

where $m_1$ is the minimum magnitude earthquake, $Q$ is the aftershock productivity, $\alpha$ describes aftershock generation efficiency, $N(r, t)$ is the aftershock rate as a function of distance and delay time from the triggering event, $c$ and $p$ are Omori's law parameters, and $q$ is the distance decay constant. The magnitude of background events, or triggered events, is a random variable drawn from the Gutenberg–Richter (G–R) distribution:

$$N(\ge m) = 10^{a-bm}, \tag{3}$$

where $a$ is related to the total number of earthquakes, and $b$ (the $b$ value) describes the relative numbers of larger events compared with smaller events. In practice, for computer simulations, $m_r$ (individual magnitude drawn from G–R distribution) is computed as:

$$m_r = m_1 - \log_{10} x_r, \tag{4}$$

where $x_r$ is a random variable drawn from the uniform distribution between $10^{(m_1-m_2)}$ and 1. For the model here, we use $m_1 = 1.5$ and $m_2 = 7.0$, which correspond to the magnitude of completeness and largest earthquake in the catalog.

Recent studies suggest that $\alpha = b = 1$ (used in this study) produces self-similar behavior, for which the increased triggering caused by larger magnitude events is compensated by their decreased numbers in the G–R relation (SHEARER 2012a). For the self-similar triggering case, the branching ratio that describes the average number of first generation aftershocks to the number of background events is

$$n = Qb \ln(10)(m_2 - m_1) \tag{5}$$

and $n = 0.39$ for the case of $m_1 = 1.5$ and $m_2 = 7.0$ in order to satisfy Båth's law (BATH 1965), i.e., that the magnitude difference between the mainshock and the largest aftershock is, on average, 1.2.

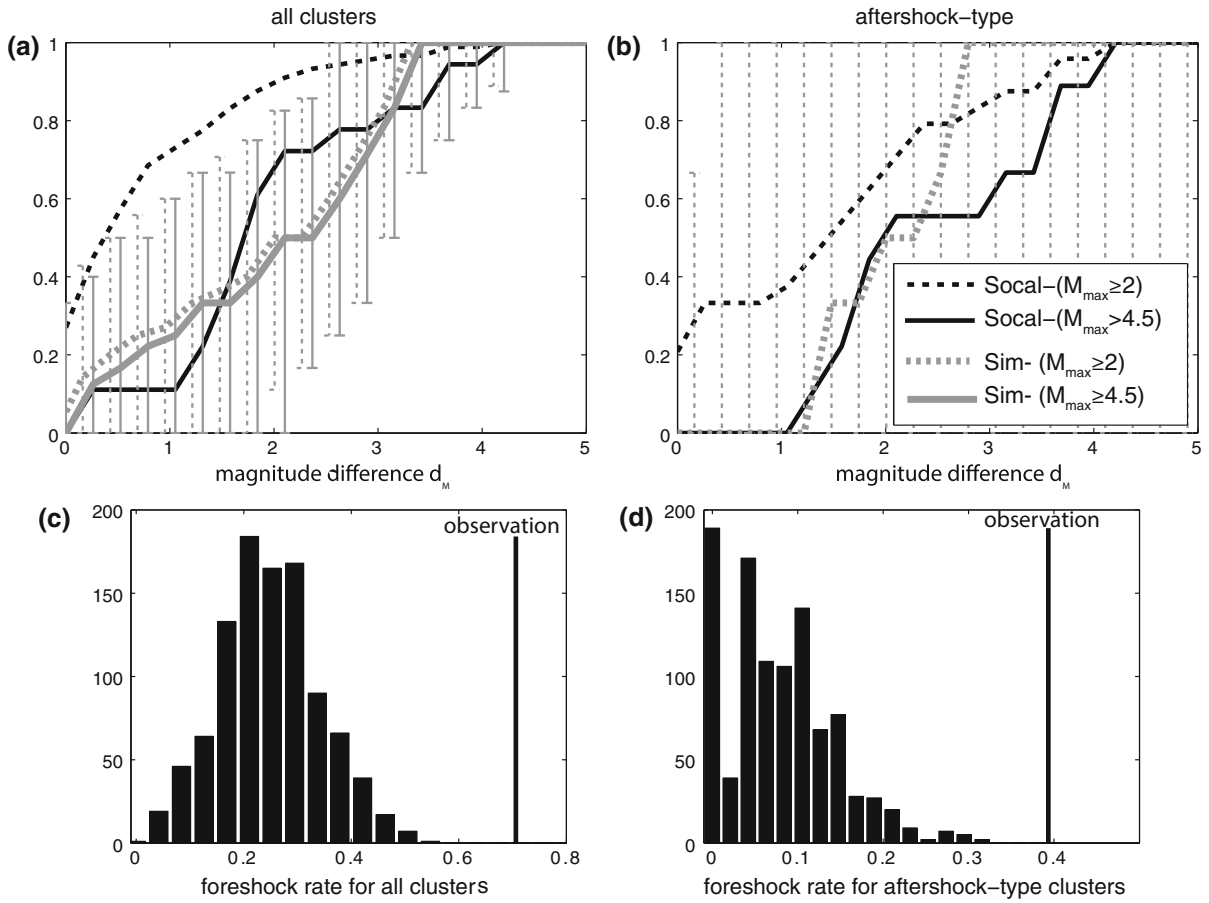


Figure 13

*Top* magnitude difference between mainshock and largest foreshock. **a** All cluster types (both aftershock-type and swarm-type); **b** only aftershock-type clusters. In both **a** and **b**, *solid lines* $M_{\max} \geq 4.5$; *dashed lines* all $M_{\max}$ ($M_{\max} \geq 2$). *Grey* synthetic catalogs, *black* observations. *Error bars* are 5 and 95 % percentiles from 1000 synthetic catalogs, line styles match corresponding data types. In **a**, the distribution that includes small mainshocks ($M_{\max} \leq 4.5$) is clearly above the 95 % limit from synthetic catalogs, thus is significantly different from synthetic catalogs. In **b**, the long *vertical dashed lines* indicate that the distribution of $d_m$ from synthetic catalogs is considerably variably due to the small number of clusters; the *grey solid line* is not applicable due to small number of clusters from synthetic catalogs. *Bottom* foreshock occurrence rate from observations and synthetic catalogs. **c** Foreshock occurrence rate for all clusters, including swarm-type clusters; **d** foreshock occurrence rate only considering aftershock-type clusters. *Vertical lines* are observations (66 % for all clusters, and 39 % for only aftershock-type clusters, these are the results from general cluster search, and differs from the 53 % for only $M \geq 5$ mainshocks), note the observed foreshock occurrence rate for with and without swarm-type clusters is significantly higher than in synthetic catalogs

For the spatial–temporal decay, we use $c = 0.001$ days, $p = 1$ and $q = 1.0$. The $p$ and $c$ values are consistent with Shearer (2012b), the $q$ value is slightly lower than the 1.37 used in Shearer (2012b), but does not strongly affect the results. We generate synthetic catalogs using the declustered southern California catalog with all events $M \geq 1.5$. The declustering process follows Reasenberg (1985), where each aftershock sequence is replaced by a single equivalent event (the mainshock), and the residual catalog approximates a Poisson process. We generate 1000 synthetic catalogs using the declustered catalog as "parent" earthquakes (background seismicity), and generate triggered aftershocks using the above relationships. The synthetic catalogs are then processed the same way as we did for the real catalogs.

On average, only 20 % of the $M \geq 5$ mainshocks in the synthetic catalogs have foreshocks, and the probability of observing a 53 % foreshock occurrence rate among our 70 mainshocks is only 3 % (based on a Gaussian distribution of the occurrence rate from the 1000 synthetic catalogs). Next, we examine

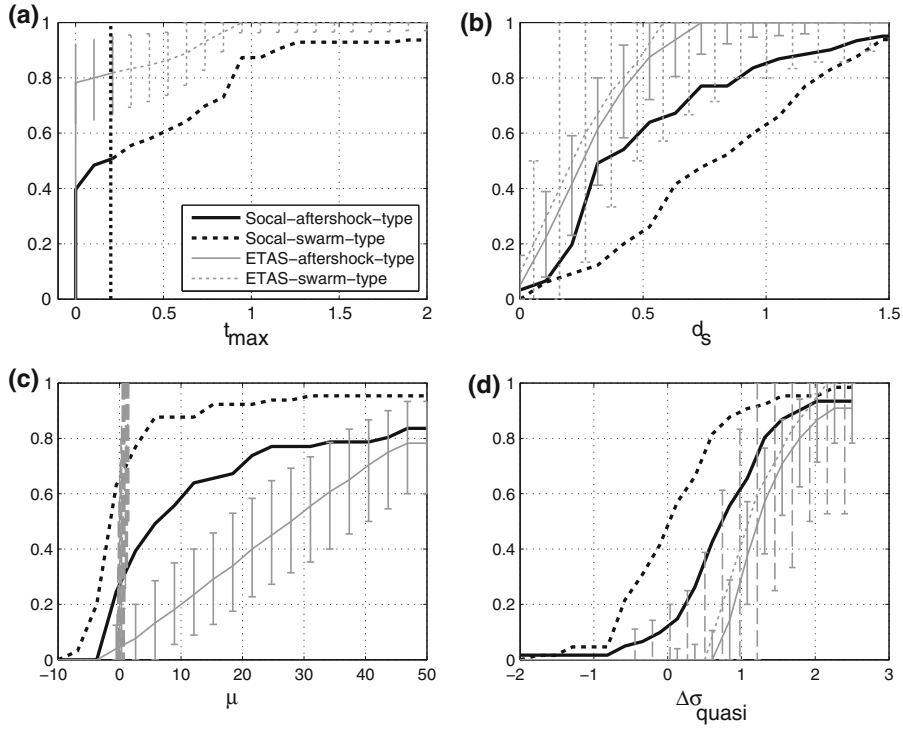


Figure 14

Comparison of distributions of different parameters between observations and synthetic catalogs for southern California. In all figures: *solid lines* aftershock-type, *dashed lines* swarm-type. *Grey* synthetic catalogs, *black* observations. *Vertical error bars* correspond to the 5 and 95 % percentiles from 1000 synthetic catalogs. **a**–**d** Correspond to the four parameters discussed in text: $t_{\max}$, $d_s$, $\mu$, $\Delta\sigma_{\text{quasi}}$. In all cases, the *dashed line* (for swarm-type) is significantly outside the variability limit from synthetic catalogs, while the *black line* is sometimes within model limits except the parameter $\mu$ that describes the moment release time history

seismicity clusters in the synthetic catalogs, as defined and described for the data in the previous section. We compare the CDF distribution of the four parameters of Chen *et al.* (2012) with observations from the southern California YHS catalog, i.e., the timing of the largest event $t_{\max}$, the skew $\mu$ of moment release history, the normalized distance between the first and second halves of the cluster $d_s$, and the effective stress drop $\Delta\sigma_{\text{quasi}}$. The results are shown in Figs. 14 and 13, and may be summarized as follows:

1. Small random clusters are common in synthetic catalogs, and about 70 % of small clusters do not grow into large clusters, which is consistent with observations.
2. The synthetic catalogs are dominated by aftershock-type clusters, and the probability of getting the observed foreshock occurrence rate is less than 5 % (based on a Gaussian distribution of the foreshock occurrence rate from 1000 synthetic catalogs), suggesting that the synthetic catalogs and observations are statistically different in terms of foreshock occurrence (see Fig. 13c, d).
3. The magnitude difference ($d_m$) between foreshocks and mainshocks for clusters with $M_{\max} \geq 4.5$ are overall consistent with observations within the model variability (see Fig. 13a), and the distribution of aftershock-type clusters is considerably variable due to the small number of clusters. The distribution of $d_m$ for all clusters with $M_{\max} \geq 2$ is statistically different from the synthetic catalogs, suggesting that the smaller events may not follow the same triggering processes as larger events (see Fig. 13a, b).
4. For the two parameters that describe the spatial evolution of rupture area ($d_s$ and $\Delta\sigma_{\text{quasi}}$), the distributions for swarm-type and aftershock-type

clusters are indistinguishable in the synthetic catalog, while observations find swarm-type clusters have higher $d_s$ and lower $\Delta\sigma_{\text{quasi}}$. This suggests that the gradual spatial expansion observed for "swarmy" clusters is not produced from triggering models with a pure power-law spatial–temporal decay (see Fig. 14b, d).

5. The skew of moment release history agrees with the temporal distribution of magnitude. The synthetic catalogs have different distributions between swarm-type and aftershock-type clusters, which is consistent with observations. The exact forms of the CDFs differ from observations, perhaps due to regional diversities of triggering parameters (see Fig. 14c).
6. 8 % of the synthetic catalogs (81 out of 1000 catalogs) have at least 3 clusters with more than 3 foreshocks (the minimum number to estimate foreshock area) and find a strong correlation between $F_{\text{area}}$ and $N_{\text{fore}}$, suggesting that the observed correlation could be reproduced from simulation by random chance. The correlation between $F_{\text{area}}$ and $M_{f\max}$ is less statistically significant.

These results depend to some extent on the parameter choices for our triggering model. One could increase the clustering and the number of foreshocks in the synthetic catalogs by increasing the aftershock productivity $Q$. However, as discussed in Shearer (2012a, b) this would result in catalogs that violate Bath's law, and, at larger values of $Q$, runaway explosions of seismicity. In any case, even if the number of clusters and foreshocks in the synthetic catalogs could be increased, the synthetic clusters would not show the spatial evolution and temporal skewness distributions of our observed clusters.

Overall, comparisons between synthetic catalogs and observations in southern California suggests that the "swarmy" features in the real catalog are not well reproduced from ETAS-like simulations. The foreshock occurrence rate is too low to be consistent with observations, and the distributions of the magnitude difference between mainshocks and foreshocks is statistically different from observations for small mainshocks. This is consistent with results documented by Shearer (2012b) for $M$ 2.5 to 5.5 mainshocks in southern California, in which the foreshock-to-aftershock ratio is observed to be too large to be consistent with Båth's law, and suggests that the observed foreshock rate cannot be explained entirely with earthquake-to-earthquake triggering models with expected rates of aftershock productivity.

## 5. Discussion and Conclusions

Our analysis approach is similar to the Vidale and Shearer (2006) study of earthquake "bursts", which considers the relative independence of the clusters from other mainshocks. Although this approach may miss some events due to the selection criteria, the earthquakes selected should represent background activity that is largely free of stress changes and other transient effects from larger events. Our foreshock statistics are generally consistent with previous observations (e.g., Abercrombie and Mori 1996) and indicate that foreshock occurrence rates: (1) depend on faulting type, mainshocks in a transtension setting tend to have more foreshocks compared with mainshocks in a transpression regime; (2) depend on mainshock depth, shallow mainshocks tend to have more foreshocks. We observe this behavior for both retrospective searches of foreshocks of $M \geq 5$ earthquakes, and prospective searches of random clusters. The dependence of clustering type on focal mechanism was also noted in our study focusing on crustal "bursts" (Chen *et al.* 2012); however, the depth dependence was not explored in that study, as the majority of "bursts" occur at shallow depth.

The observed faulting type and depth dependence is consistent with theories related to stress loading during earthquake cycle, where the loading style depends on the regional stress field (Sibson 1993). For pure normal faults, a "loading-weakening" mechanism, where the shear strength reduces with stress loading, is expected; while for reverse faults, a "loading-strengthening" mechanism is expected. For strike–slip faults, depending on the actual stress values, both mechanisms are possible, in which the style changes progressively from "loading-weakening" to "loading-strengthening" as faulting type changes from transtension to transpression status. If the mean

stress decreases during shear loading, it is more likely for fluid to flow into the fault zone, which may facilitate the occurrence of small events. Abercrombie and Mori (1996) noted that increased normal stress is commonly expected for reverse faulting and deeper events, which may prohibit occurrence of small events.

The high foreshock occurrence rate from the "burst" approach (53 % for $M \geq 5$ mainshocks, 66 % for all clusters without a magnitude requirement) raises questions about the predictive value of foreshock activities. We investigate the relationship between various foreshock parameters and mainshock magnitude, and find that:

1. Among all the foreshock parameters (number of foreshocks, area of foreshocks, foreshock magnitude), only the number of foreshocks is weakly correlated with mainshock magnitude for carefully selected $M \geq 5$ mainshocks, and does not apply to our generalized cluster search (in Sect. 3) without a mainshock magnitude requirement.
2. For $M \geq 5$ earthquakes, comparing with Dodge *et al.* (1996), the foreshock areas for the "new" mainshocks (in this study) do not fall along the scaling relationship between nucleation zone and mainshock size (see Fig. 7), and the correlation is not statistically significant. There is no significant correlation between foreshock area and mainshock size.
3. A stronger correlation is seen between area and the magnitude of the largest foreshock; however, it also is not valid for smaller mainshocks ($M \leq 4.5$). This is consistent with results in Felzer *et al.* (2004), in which they argue that this agrees with a single-mode triggering process for foreshocks for the larger events, although this may not apply to small events (e.g., $M_{\max} \leq 4.5$) based on observations here.
4. The most consistent correlation for all sized mainshocks is between foreshock area and the number of foreshocks. About 8 % of the synthetic catalogs based on self-similar triggering produce such a correlation; however, the percentage is not statistically significant. Such a correlation confirms the "swarmy" nature of foreshock sequences, where each event may nucleate near the edge of the rupture zone of preceding events, consistent with a self-organized earthquake sequence based on a spring-block model (Hainzl and Fischer 2002; Hainzl 2003), in which the same mechanical coupling system can produce the main statistical characteristics of both aftershock-type and swarm-type sequences given the appropriate parameter range. For example, the viscous-elastic block system reproduces earthquake swarms in the Vogtland region with higher viscous coupling between blocks (Hainzl 2003), and the same elastic strike–slip fault generates swarm-like sequences with a short critical slip distance ($D_c$—higher dilatancy strengthening) (Yamashita 1999). $D_c$ scales with the characteristic length of small-scale heterogeneity, and within highly fractured zones, a shorter $D_c$ is expected. The observed relationship between clustering type and faulting system is consistent with this point of view, with a higher probability of foreshock occurrence in more complex fault zones.
5. To understand what features could be explained by synthetic triggering models, we compare parameter distributions from observations with 1000 random synthetic catalogs based on a self-similar branching triggering model. The results suggest that for $M \geq 4.5$ mainshocks, the magnitude difference ($d_m$) is comparable with observations within the model variability. The inconsistencies are in the foreshock occurrence rate and parameters related to spatial expansion of individual clusters, most notably for the "swarm-type" clusters (see Figs. 13, 14). These results suggest that swarm-like behavior that is not well represented by a unified aftershock-triggering model. Accounts for heterogeneity in stress transfer parameters in catalog simulators may help to represent such features more accurately.

Overall, the observations and comparisons with synthetic catalogs suggest that foreshocks are not necessarily part of the "nucleation process" of the eventual mainshock, as there is no consistent correlation between foreshock properties and the mainshock. This also does not necessarily imply a single "rupture mode" for all sized events. Rather,

foreshocks are likely driven by independent aseismic processes occurring within the mainshock rupture zone (as suggested for interplate earthquakes Bouchon *et al.* 2013). Regardless of the initiation of the sequence, its evolution is controlled by local heterogeneity, as a unified triggering model could not explain features observed for smaller events. Small, compact clusters are frequent in California, but only 30 % grow into larger clusters with more than 50 events. Before the eventual mainshock occurs, it is difficult to distinguish "foreshocks" from random small clusters. And even if a small cluster is recognized as containing likely "foreshocks", the eventual size of the mainshock is difficult to predict.

This imposes challenges to utilizing the predictive value of foreshocks and in creating simulated catalogs that account for the "swarmy" foreshock features. An important step is to focus more on the role of microearthquakes, as a recent literature review suggested (Mignan 2014), and incorporate spatial variations of earthquake triggering parameters. Based on the current analysis in California, the following properties may be particularly useful: (1) with a unified magnitude cutoff, the number of foreshocks correlates with mainshock magnitude for large earthquakes ($M \geq 5$); (2) the identified foreshocks for $M \geq 5$ mainshocks are localized within the "Mogi" zones prior to the mainshock, and are mostly associated with localized fault discontinuities (Jones 1984; Chen and Shearer 2013); (3) the foreshock occurrence patterns are consistent with earthquake clustering patterns. For example, in the Eastern California Shear Zone, where most mainshocks have foreshocks, there is a 20 % chance that a larger earthquake may occur following a small compact cluster (for southern California, 60 out of 311 clusters grow into larger clusters that do not start with the mainshock). The Hector Mine earthquake occurred within zones of enhanced swarm activities following the Landers earthquake, and is immediately preceded by a cluster of 18 events (Chen and Shearer 2013). Increased "swarmy" activity in a "seismic gap" area or near long fault segments may indicate a potential larger earthquake. Moreover, in several cases, foreshocks exhibit spatial migration (e.g., the Tohoku earthquake Kato *et al.* 2012 and the Chile earthquake Kato and Nakagawa 2014), and spectral differences from background seismicity (Chen and Shearer 2013). Thus, if historic incidences of foreshocks are well documented, then repetitive occurrence of similar clusters in similar tectonic settings may indicate future mainshocks.

## *Acknowledgments*

We thank the Northern California Seismic Network, the U.S. Geological Survey, Menlo Park, and the Berkeley Seismological Laboratory, University of California, Berkeley for providing a moment tensor catalog. We thank the Global CMT Project for providing moment tensor solutions. We thank Richard Sibson for discussion on precursory behavior based on stress analysis. The maps are generated using the GMT software package.

## References

Abercrombie, R. E., and J. Mori (1996), *Occurrence patterns of foreshocks to large earthquakes in the western united states*, Nature, *381*(6580), 303–307.

Bath, M. (1965), *Lateral inhomogeneities of upper mantle*, Tectonophysics, *2*(6), 483.

Beroza, G. C., and W. L. Ellsworth (1996), *Properties of the seismic nucleation phase*, Tectonophysics, *261*(1–3), 209–227, doi:10.1016/0040-1951(96)00067-4.

Bouchon, M., V. Durand, D. Marsan, H. Karabulut, and J. Schmittbuhl (2013), *The long precursory phase of most large interplate earthquakes*, Nature Geosci, *6*, 299–302, doi:10.1038/ngeo1770.

Chen, X., and P. Shearer (2013), *California foreshock sequences suggest aseismic triggering process*, Geophys. Res. Lett., *40*, 2602–2607, doi:10.1002/grl.50444.

Chen, X., P. M. Shearer, and R. Abercrombie (2012), *Spatial migration of earthquakes within seismic clusters in southern California: Evidence for fluid diffusion*, J. Geophys. Res., *117*(B04301), doi:10.1029/2011JB008973.

Dodge, D. A., G. C. Beroza, and W. L. Ellsworth (1996), *Detailed observations of California foreshock sequences: Implications for the earthquake initiation process*, Journal of Geophysical Research-Solid Earth, *101*(B10), 22,371–22,392.

Ellsworth, W. L., and G. C. Beroza (1995), *Seismic evidence for an earthquake nucleation phase*, Science, *268*(5212), 851–855, doi:10.1126/science.268.5212.851.

Felzer, K. R., R. E. Abercrombie, and G. Ekstrom (2004), *A common origin for aftershocks, foreshocks, and multiplets*, Bulletin of the Seismological Society of America, *94*(1), 88–98, doi:10.1785/0120030069.

Hainzl, S., and T. Fischer (2002), *Indications for a successively triggered rupture growth underlying the 2000 earthquake swarm in vogtland/nw bohemia*, Journal of Geophysical Research-Solid Earth, *107*(B12), 2338, doi:10.1029/2002jb001865.

Hainzl, S. (2003), *Self-organization of earthquake swarms*, Journal of Geodynamics, *35*(1–2), 157–172.

Hardebeck, J. L., and P. M. Shearer (2003), *Using s/p amplitude ratios to constrain the focal mechanisms of small earthquakes*, Bulletin of the Seismological Society of America, *93*(6), 2434–2444.

Hauksson, E., W. Yang, and P. M. Shearer (2012), *Waveform relocated earthquake catalog for southern California (1981 to june 2011)*, Bulletin of the Seismological Society of America, *102*(5), 2239–2244, doi:10.1785/0120120010.

Helmstetter, A., D. Sornette, and J. R. Grasso (2003), *Mainshocks are aftershocks of conditional foreshocks: How do foreshock statistical properties emerge from aftershock laws*, Journal of Geophysical Research-Solid Earth, *108*(B1), 24, doi:10.1029/2002jb001991.

Helmstetter, A., Y. Y. Kagan, and D. D. Jackson (2005), *Importance of small earthquakes for stress transfers and earthquake triggering*, Journal of Geophysical Research-Solid Earth, *110*(B5), 13, doi:10.1029/2004jb003286.

Jones, L. M. (1984), *Foreshocks (1966-1980) in the San-Andreas system, California*, Bulletin of the Seismological Society of America, *74*(4), 1361–1380.

Kato, A., and S. Nakagawa (2014), *Multiple slow-slip events during a foreshock sequence of the 2014 Iquique, Chile mw8.1 earthquake*, Geophysical Research Letters, *41*, doi:10.1002/2014GL061138.

Kato, A., K. Obara, T. Igarashi, H. Tsuruoka, S. Nakagawa, and N. Hirata (2012), *Propagation of slow slip leading up to the 2011 m-w 9.0 tohoku-oki earthquake*, Science, *335*(6069), 705–708, doi:10.1126/science.1215141.

Mogi, K. (1963), *Some discussions on aftershocks, foreshocks and earthquake swarms - the fracture of a semi-infinite body casued by an inner stress origin and its relation to the earthquake phenomena*, Bulletin of the Earthquake Research Institute, *41*, 615–658.

McGuire, J. J., M. S. Boettcher and T. H. Jordan (2005), *Foreshock sequences and short-term earthquake predictability on East Pacific Rise transform faults*, Nature, *434*.

Mignan, Arnaud (2014), *The debate on the prognostic value of earthquake foreshocks: A meta-analysis*, Scientific reports, *4*(4099), doi:10.1038/srep04099.

Ogata, Y. (1999), *Seismicity analysis through point-process modeling: A review*, Pure and Applied Geophysics, *155*(2–4), 471–507.

Reasenberg, P. (1985), *Second-order moment of central California seismicity*, J. Geophys. Res., *90, pp. 5479–5495*.

Reasenberg, P. (1999), *Foreshock occurrence before large earthquakes*, J. Geophys. Res., *104*(B3), 4755–4768.

Shearer, P. M. (2009), *Introduction to Seismology*, second edition, Cambridge University Press.

Shearer, P. M., and G. Q. Lin (2009), *Evidence for mogi doughnut behavior in seismicity preceding small earthquakes in southern California*, Journal of Geophysical Research-Solid Earth, *114*(B01318), doi:10.1029/2008jb005982.

Shearer, P. M., G. A. Prieto, and E. Hauksson (2006), *Comprehensive analysis of earthquake source spectra in southern California*, Journal of Geophysical Research-Solid Earth, *111*(B06303), doi:10.1029/2005jb003979.

Shearer, P. M. (2012a), *Self-similar earthquake triggering, Båth's law, and foreshock/aftershock magnitudes: Simulations, theory, and results for southern California*, J. Geophys. Res., *117*(B06310), doi:10.1029/2011jb008957.

Shearer, P. M. (2012b), *Space-time clustering of seismicity in California and the distance dependence of earthquake triggering*, J. Geophys. Res., *117*(B10306), doi:10.1029/2012JB009471.

Sibson, R. H. (1993), *Load-strengthening versus load-weakening faulting*, J. Struct. Geol., *15*(2), 123–128.

Toda, S., R. S. Stein, G. C. Beroza, and D. Marsan (2012), *Aftershocks halted by static stress shadows*, Nature Geosci, *5*(410–413), doi:10.1038/ngeo1465.

Vidale, J. E., and P. M. Shearer (2006), *A survey of 71 earthquake bursts across southern California: Exploring the role of pore fluid pressure fluctuations and aseismic slip as drivers*, Journal of Geophysical Research-Solid Earth, *111*(B05312), doi:10.1029/2005jb004034.

Waldhauser, F., and D. P. Schaff (2008), *Large-scale relocation of two decades of northern California seismicity using cross-correlation and double-difference methods*, J. Geophys. Res., *113*(B08311), doi:10.1029/2007JB005479.

Yamashita, T. (1999), *Pore creation due to fault slip in a fluid-permeated fault zone and its effect on seismicity: Generation mechanism of earthquake swarm*, Pure and Applied Geophysics, *155*(2–4), 625–647.

Yang, W., E. Hauksson, and P. M. Shearer (2012), *Computing a large refined catalog of focal mechanisms for southern California (1981–2010): Temporal stability of the style of faulting*, Bulletin of the Seismological Society of America, *102*(3), pp. 1179–1194, doi:10.1785/0120110311.

(Received August 28, 2014, revised May 4, 2015, accepted May 7, 2015)